PCCP

Accepted Manuscript

This article can be cited before page numbers have been issued, to do this please use: M. Paskevicius, M. B. Ley, D. A. Sheppard, T. R. Jensen and C. Buckley, *Phys. Chem. Chem. Phys.*, 2013, DOI: 10.1039/C3CP53920B.

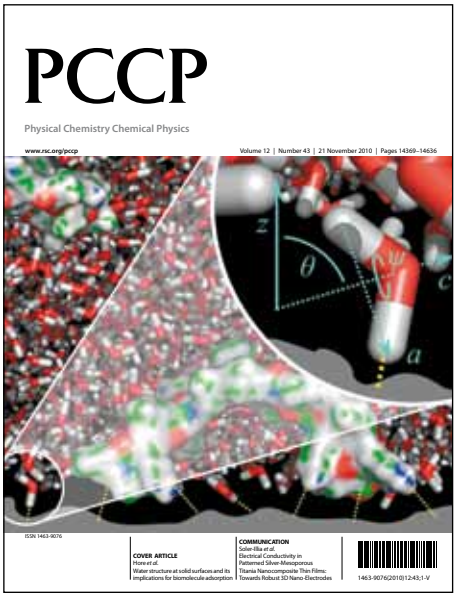

This is an *Accepted Manuscript*, which has been through the RSC Publishing peer review process and has been accepted for publication.

Accepted Manuscripts are published online shortly after acceptance, which is prior to technical editing, formatting and proof reading. This free service from RSC Publishing allows authors to make their results available to the community, in citable form, before publication of the edited article. This *Accepted Manuscript* will be replaced by the edited and formatted *Advance Article* as soon as this is available.

To cite this manuscript please use its permanent Digital Object Identifier (DOI®), which is identical for all formats of publication.

More information about *Accepted Manuscripts* can be found in the **Information for Authors**.

Please note that technical editing may introduce minor changes to the text and/or graphics contained in the manuscript submitted by the author(s) which may alter content, and that the standard **Terms & Conditions** and the **ethical guidelines** that apply to the journal are still applicable. In no event shall the RSC be held responsible for any errors or omissions in these *Accepted Manuscript* manuscripts or any consequences arising from the use of any information contained in them.

View Article Online
DOI: 10.1039/C3CP53920B

Different Melting and Decomposition Mechanisms

317x317mm (96 x 96 DPI)

PCCP

RSCPublishing

ARTICLE

Eutectic Melting in Metal Borohydrides

Cite this: DOI: 10.1039/xoxxoooooox

Mark Paskevicius,[*a] Morten B. Ley,[a,b] Drew A. Sheppard,[a] Torben R. Jensen[b] and Craig E. Buckley[a]

Received ooth January 2012,
Accepted ooth January 2012

DOI: 10.1039/xoxxoooooox

www.rsc.org/

A series of monometallic borohydrides and borohydride eutectic mixtures have been investigated during thermal ramping by mass spectroscopy, differential scanning calorimetry, and photography. Mixtures of $LiBH_4$-$NaBH_4$, $LiBH_4$-KBH_4, $LiBH_4$-$Mg(BH_4)_2$, $LiBH_4$-$Ca(BH_4)_2$, $LiBH_4$-$Mn(BH_4)_2$, $NaBH_4$-KBH_4, and $LiBH_4$-$NaBH_4$-KBH_4 all displayed melting behaviour below that of the monometallic phases (up to 167 °C lower). Generally, each system behaves differently with respect to their physical behaviour upon melting. The molten phases can exhibit colour changes, bubbling and in some cases frothing, or even liquid-solid phase transitions during hydrogen release. Remarkably, the eutectic melt can also allow for hydrogen release at temperatures lower than that of the individual components. Some systems display decomposition of the borohydride in the solid-state before melting and certain hydrogen release events have also been linked to the adverse reaction of samples with impurities, usually within the starting reagents, and these may also be coupled with bubbling or frothing of the ionic melt.

1. Introduction

There has been much interest in eutectic salt mixtures for well over a century, ever since early investigations into electrolysis by Faraday in the mid-1800's [1]. Research into molten salts has led to the development of an array of applications and niche industries that can make use of their physical properties in the molten state. Molten salt systems are known as ionic liquids when the melting point is below 100 °C. They can be utilized as reaction media [2], and as such, there has been considerable research into the solubility and reactivity of dissolved substances within these melts [3]. Certain extractive metallurgy operations implement molten salts in the electrolytic winning of target metals, such as aluminum or magnesium at elevated temperatures [4]. In addition, molten salts are now taking on a major role in solar thermal energy storage as sensible heat and latent heat phase change materials [5]. The nature of molten salt systems is also important in understanding the high temperature behavior of many hydrogen storage materials. For example, metal borohydrides (or tetrahydroborates) are pursued in the hydrogen storage field because of their high gravimetric hydrogen densities, but they often undergo a transition to a molten state before releasing hydrogen [6, 7].

There is still active research into understanding the nature of the structural changes that occur during crystal melting, including in pure alkali metal halide systems [8]. A pure alkali halide liquid can be conceptualized as consisting of small domains of regular crystal-type arrays undergoing dynamic structural reorganization [9]. There is also evidence for reductions in the average coordination number upon melting (i.e. from six to four) coupled by reductions in the internuclear distances of the salt [2, 3]. Understanding eutectic melting is more complicated, where a two (or more) component system can maintain a liquid state below the melting points of its pure constituents (Figure S1A). Eutectic melting involves the participation of additional domains to that of a pure salt, in-fact, having regular structures characteristic of double salts [9]. Solid solutions between phase mixtures can also form, where a common structure exists, containing random distributions of ions on the same crystallographic position (Figure S1B). Eutectics are generally formed when the various ion constituents (anion or cation) have significantly different sizes and/or charge, whilst if these sizes and charges are comparable then these mixtures are more likely to form solid solutions [9].

Eutectics in simple hydride-halide compositions have been well characterized since the 1960's. For example, LiH-halide systems are well-studied with respect to the pure compound's melting point of 686.4 °C (under 1 bar H_2) [10]. The eutectic for LiH-Li*X* (*X* = Cl, Br and I), and LiH-NaCl were found to be at 495.6 °C (76 mol% LiCl) [10], 400 °C (71 mol% LiBr) [11], 390.8 °C (70.3 mol% LiI) [10], and 565.7 °C (44.8 mol% NaCl) [12] with no solid solutions observed. In contrast, LiH-LiF mixtures exhibit solid solution formation in all compositions, and only a minor decrease in melting temperature (4.5 °C) from LiH was detected at 13 mol% LiF [13] (Figure S1B). Similar solid solution behavior exists for KBH_4-KCl, which has been shown to exhibit a slightly reduced melting point at 590 °C (at ~70 mol% KBH_4) [14, 15].

There is also the possibility of double salt compounds being formed in certain binary salt systems in addition to eutectic formation. This can occur in alkali metal salts where cation mixtures have the greatest size differences (i.e. $LiCsX_2$ or $LiRbX_2$) [9]. The presence of double salts can alter the phase diagram and affect the ideal eutectic behavior of the system (Figure S1C). The double salts can result in peritectic points in the phase diagram due to their higher melting temperature than the ideal eutectic point. There are a range of dual cation salts that have been reported in the borohydride literature that may influence their respective phase diagrams, resulting in shallower melting temperatures. Some of these dual cation compounds include $KSc(BH_4)_4$ [16], $K_2Mg(BH_4)_4$, $K_2Mn(BH_4)_4$, $K_3Mg(BH_4)_5$, $KMn(BH_4)_3$ [17], $LiZn_2(BH_4)_5$, $NaZn_2(BH_4)_5$, and $NaZn(BH_4)_3$ [18]. Mixed-anion mixed-cation compounds may also form either fully ordered structures e.g. $KZn(BH_4)Cl_2$ [19], $LiM(BH_4)_3Cl$ (M = La, Ce, Gd) [20-22] or partly disordered structures, $NaY(BH_4)_2Cl_2$ [23]. Anion substitution in metal borohydrides can also occur because the complex borohydride ion may resemble the halide ions in the solid state. For example, halide stabilized lithium borohydride ($LiBH_4$–LiX, X = Cl, Br, I) [24-27] forms solid solutions, $Li(BH_4)_{1-y}X_y$, which tend to stabilize the hexagonal $LiBH_4$ polymorph at lower temperatures as compared to the transition temperature (~110 °C).

The melting behavior of metal borohydrides is more complex than for similar alkali metal halide salt systems, especially when mixed with other metal borohydrides or metal halides. The metal borohydride may decompose during thermal treatment often during or shortly after melting [28]. Hydrogen release from a metal borohydride may be a complex polymerization process with many possible intermediates [29]. This decomposition is controlled by both thermodynamic and kinetic factors. Therefore, decomposition can occur at any temperature where the hydrogen gas pressure is below the equilibrium pressure for the system, and when there is significant energy to overcome kinetic barriers. It is because of these thermodynamic and kinetic barriers that the hydrogen backpressure is a critical factor in controlling the decomposition temperature of a borohydride. Experimental studies into the effect of backpressure on borohydride decomposition suggest that it plays a role in determining reaction pathways [30]. Restricting decomposition to higher temperatures can alter the behavior of the borohydride system and melting events or even phase transformations may be observable, where they would not be under vacuum or atmospheric pressures. The $NaBH_4$-NaH system was investigated in 1966 and an eutectic was determined at 395 °C (at 21 mol% NaH) [31]. The effect of hydrogen backpressure upon the decomposition of a range of $NaBH_4$-NaH mixtures was investigated in this study, where the pressure had no effect on melting temperatures but higher backpressures restricted decomposition to higher temperatures. A metal borohydride can be prepared by reacting a metal hydride with borane gas (i.e. diborane, B_2H_6) [32, 33], which indicates that borane (i.e. BH_3) could take part in certain decomposition processes as well. This may explain the observation of a variety of higher boranes as decomposition products, which could be formed by polymerization reactions [34, 35].

There are many reports in the literature of containment problems with borohydrides after melting has occurred. Molten borohydrides have been known to bubble, froth, vaporize, spatter, and even climb vessel walls [28, 36, 37]. This phenomenon is not unique to borohydrides. It is well known that metal hydrides can be used to generate bubbles and frothing in molten aluminum to produce porous aluminum after cooling [38]. Just above its melting point aluminum has a lower viscosity than typical molten salts, but a much higher surface tension (see Table S1). Vigorous frothing has been observed in molten salt systems, such as the $LiCl$-Li_2CO_3 system, attributed to dissolved gases, but could result from decomposition and CO_2 evolution [39]. In addition, effervescence was reported to occur in certain $NaBF_4$ melts resulting from BF_3 gas evolution [40]. Thus, it is apparent that gas evolution within a molten phase can cause frothing, given that the phase has favorable physical properties.

The physical properties of molten borohydride mixtures are not well known, however there is considerable data on the properties of binary alkali halide salt mixtures, including their eutectic compositions (see Table S1) [41]. The viscosity of a molten salt of eutectic composition just above its melting point is typically noticeably higher than that of its constituents, possibly due to the lower melting temperature. These viscosities are relatively low, close to that of water, especially when compared to more viscous compounds such as $SiCl_4$ or glycerol. In contrast, the surface tension of molten salts and their mixtures are quite high. Surface tensions for typical liquids at room temperature lie much lower than these, including water, $SiCl_4$, or glycerol, with the exception of Hg. The surface tension is a key parameter in the formation of froth in gas-liquid mixtures, where high surface tension leads to larger, but less stable bubbles [42]. In fact, surface tension and the fluid density have been identified to have the most significant impact on froth structure, with some dependence on viscosity [43]. However, there is also a significant impact on froth formation and lifetime with temperature and gas overpressure [44], although studies of this nature are sparse [45].

Several metal borohydride and amide systems are considered as solid or liquid electrolytes for lithium batteries [46]. A modern day battery is made up of electrochemical cells. Each cell consists of a positive and a negative electrode (both sources of chemical reactions) separated by an electrolyte solution containing dissociated salts, which enable ion transfer between the two electrodes. Solid electrolytes have the potential to replace liquid electrolytes and thereby improve the safety of next-generation high-energy batteries. Hexagonal $LiBH_4$ (T > 110 °C) and the hexagonal halide stabilized polymorphs h-$Li(BH_4)_{1-y}X_y$, (X = Cl, Br, I), were found to have very high lithium ion conductivities in the range 10^{-5} to 10^{-4} Scm^{-1} at room temperature, which increase to about 10^{-2} Scm^{-1} at 150 °C [47]. Mixed borohydride amide systems $Li(BH_4)(NH_2)$ and $Li_4(BH_4)(NH_2)_3$ both have a ionic conductivities of 2×10^{-4}

Scm^{-1} at room temperature, that increases to 1×10^{-4} Scm^{-1} at ~100 °C, where the compounds melt [48]. High Li ion conductivity has also been observed for the mixed-anion mixed-cation compounds systems $LiM(BH_4)_3Cl$ (*M* = La, Ce, Gd). The crystal structure of $LiM(BH_4)_3Cl$ facilitates the observed high Li ion conductivity of 1.0×10^{-4} Scm^{-1} at 20 ºC, as the tetranuclear anionic clusters of $[M_4Cl_4(BH_4)_{12}]^{4-}$ (*M* = La, Ce, Gd) are charge balanced by disordered Li^+ ions, occupying 2/3 of the available positions in the crystal lattice allowing them to move within the structure. For $LiLa(BH_4)_3Cl$ the conductivity increases to 1.0×10^{-3} Scm^{-1} T > 100 ºC [20, 21, 49]. The low melting temperature for the eutectic systems studied here may facilitate ionic conduction at temperatures above their reduced melting points. The systems $LiBH_4$-KBH_4 and $LiBH_4$-$NaBH_4$-KBH_4 both exhibit melting at ~110 °C and their ionic conductivity may be comparable to that of liquid $Li(BH_4)(NH_2)$.

The motive of this investigation is to explore the physical behavior of single and eutectic mixtures of borohydrides during thermal treatment to provide insight into their viability in practical applications.

2. Experimental

All sample handling was performed in an argon glovebox (< 1 ppm O_2 and H_2O). $LiBH_4$ (≥ 90 %), $NaBH_4$ (99 %), KBH_4 (99.9 %), γ-$Mg(BH_4)_2$ (95 %), and $Ca(BH_4)_2$ (> 96.5 %) were all purchased from Sigma-Aldrich and used without further purification. $Mn(BH_4)_2$ was synthesized according to a previously described procedure [17] and X-ray diffraction data is provided in Figure S2. Eutectic compositions were mixed using either hand grinding or light ball milling, performed in an Across International PQ-N04 planetary mill using a 50 mL stainless steel 304 vial and 10 mm balls (40:1 ball to powder mass ratio) at 400 rpm for 30 minutes.

Photographs were collected using a digital camera whilst typically heating samples at 10 °C/minute from room temperature to a temperature above the melting point. Samples were sealed under argon in a glass vial connected to a 1 bar blow-off valve to maintain a constant total pressure, but the partial pressure of hydrogen in the vial may increase during the experiment. A 1.59 mm stainless steel thermocouple was in contact with the sample within the glass vial to monitor temperature during thermal excursions. The glass vial was encased within an aluminum (or brass) block with open viewing windows for photography, to provide reasonably uniform heating by rod heaters, interfaced to a temperature controller. Cooling was performed by turning the temperature controller off and letting the samples slowly cool back to ambient temperature whilst embedded in the heater block (~1 hour). It should be noted that there is some thermal gradient over the sample in this configuration and it is likely that temperatures are ± 5 °C in general.

X-ray Diffraction (XRD) data were collected using a Bruker D8 Advance diffractometer (Cu-Kα1+2 radiation, λ = 1.54 Å). The instrument is equipped with a LynxEye linear position sensitive detector (PSD) with 192 pixels over 3° 2θ. Samples were enclosed within an airtight poly(methyl methacrylate) (PMMA) bubble holder.

Thermal gravimetric analysis (TGA) and differential scanning calorimetry (DSC) data was obtained simultaneously with mass spectrometry (MS) analysis of the residual gas using a PerkinElmer STA 6000 apparatus and a Hiden Analytical HPR-20 QMS sampling system. The samples (approx. 3 mg) were placed in an Al_2O_3 or Al crucible and heated from 50 to 500 °C (5 or 10 °C/min) in an argon flow of 65 mL/minute. The released gas was analyzed for hydrogen and diborane. The TGA/DSC data have sloping backgrounds in some cases that is an artifact of the measurement equipment and in some cases due to sample loss from the crucibles due to melting/frothing. Reliable TGA/DSC/MS data for the decomposition of $NaBH_4$ and KBH_4 was not able to be obtained due to the high decomposition temperature and the tendency for these materials to froth during hydrogen release.

3. Results and Discussion

A. Monometallic Borohydrides

A.1. $LiBH_4$

The melting behaviour of $LiBH_4$ is displayed in Figure 1. It has long been known that $LiBH_4$ goes through a molten phase transition at 280 °C into a clear liquid [50]. There is a well-documented minor hydrogen release upon melting $LiBH_4$ [35, 51-53]. However, this hydrogen release at 280 °C is not present in the desorption of rehydrogenated samples [53, 54] and indicates rapid adverse redox reactions of the molten phase [24] with impurities in the as-synthesized starting reagent.

Above 330 °C $LiBH_4$ begins to decompose via a complex reaction pathway [35], releasing hydrogen gas (see Figure 2). This is coupled by the formation of LiH along with a nanocrystalline $Li_2B_{12}H_{12}$ phase that also decomposes through a series of

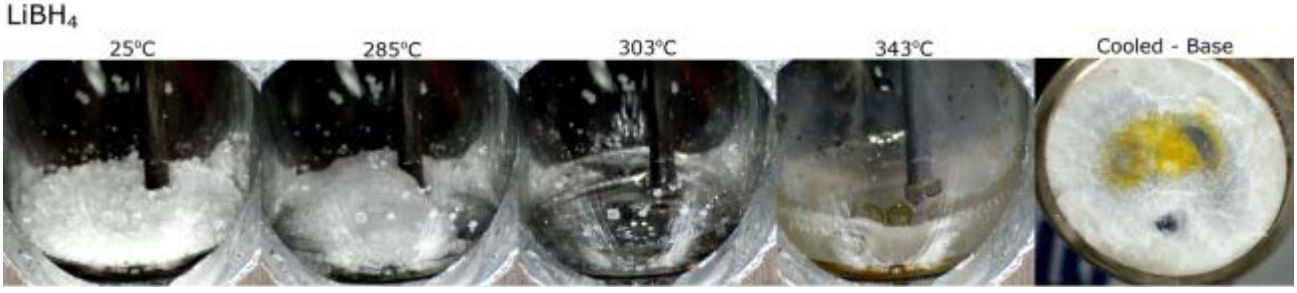

Figure 1: Photographic sequence during thermolysis of $LiBH_4$ at 10 °C/minute under argon and evolved gases maintained at 1 bar.

View Article Online
DOI: 10.1039/C3CP53920B

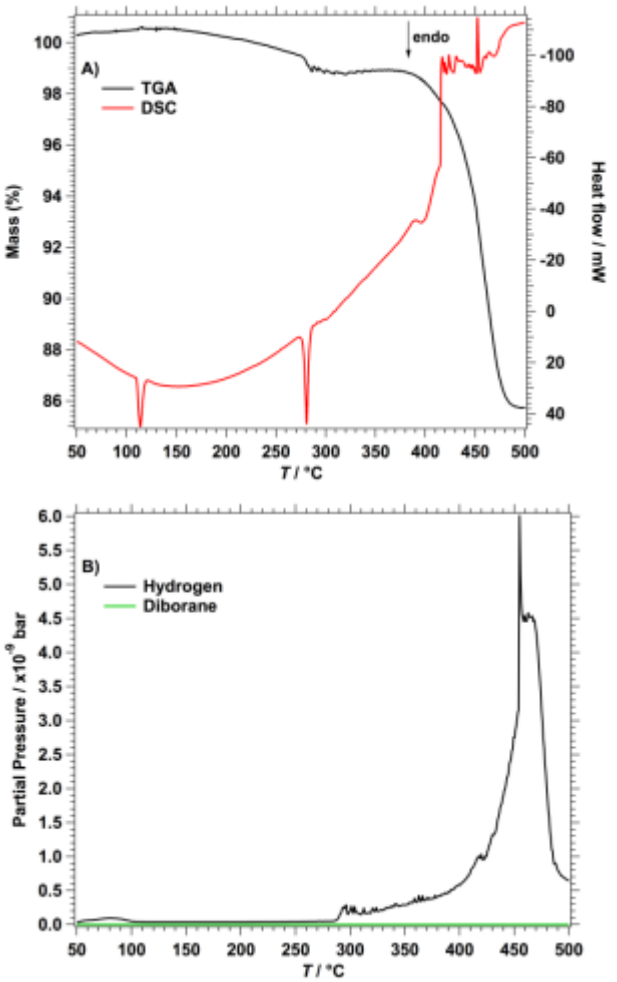

Figure 2: A) TGA, DSC and B) MS data collected simultaneously during the thermolysis of $LiBH_4$ under flowing argon.

$Li_2B_{12}H_{12-x}$ compositions [35]. These solid phases are formed from molten $LiBH_4$, causing the melt to appear cloudy. $LiBH_4$ has been observed to evaporate under vacuum conditions above its melting point, with the evolution of Li, B-H and H atoms/radicals [36]. This study also detected the condensation of these molecules on vessel walls, in a similar manner to the deposition observed here. There have also been problems in measuring hydrogen desorption from $LiBH_4$, primarily due to the molten phase climbing vessel walls and blocking filters and gas lines [35]. It is also well known that molten $LiBH_4$ reacts noticeably with glass [50], over the course of hours at elevated temperature. However this was not observed in this fast study, where $LiBH_4$ only exists in the molten state for a short period of time (on the order of minutes).

A.2. $NaBH_4$

$NaBH_4$ is known to melt at 505 °C and decompose, releasing hydrogen gas at 534 ± 10 °C under a 1 bar hydrogen back pressure [55, 56]. The behaviour of $NaBH_4$ during heating is displayed in Figure 3. The pristine white powder begins to change colour to a mottled light brown above 460 °C indicating that hydrogen desorption has begun in the solid-state. The powder begins to melt above 510 °C into a uniform transparent liquid at 530 °C. During this transition there is minor splattering of the $NaBH_4$ that results in numerous liquid droplets over the surface of the glass walls. Minor bubbling also occurs above the melting point, indicative of the slow release of hydrogen, but there is no evidence of foaming in this system. Upon quenching, the residue appears to be multi-phase where darker coloured compounds have settled to the bottom of the cell and lighter coloured compounds (likely pristine $NaBH_4$) exist on the top surface of the solid pellet.

A.3. KBH_4

KBH_4 is not as well studied as the lighter alkali metal

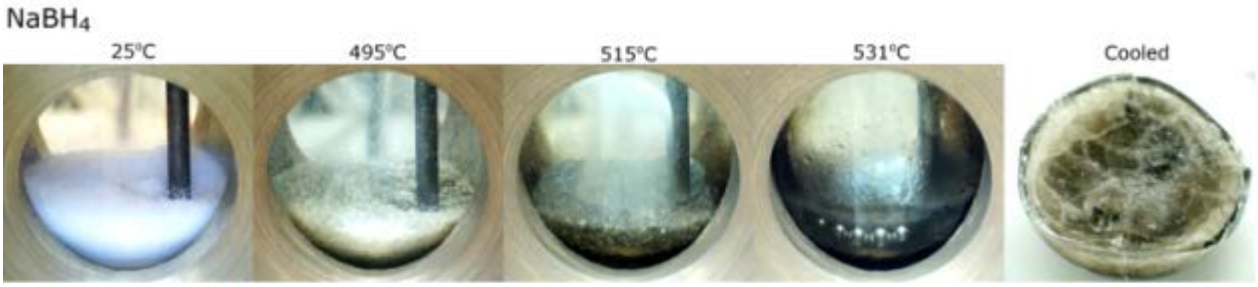

Figure 3: Photographic sequence during thermolysis of $NaBH_4$ at 10 °C/minute under argon and evolved gases maintained at 1 bar.

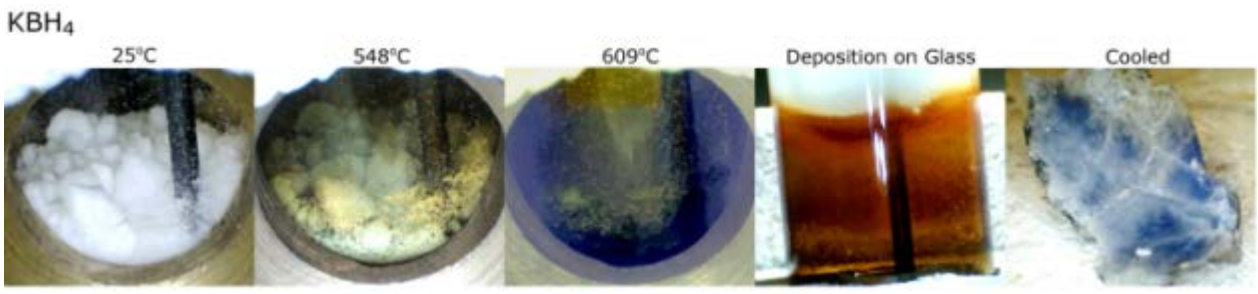

Figure 4: Photographic sequence during thermolysis of KBH_4 at 10 °C/minute under argon and evolved gases maintained at 1 bar.

borohydrides, likely due to the reportedly high hydrogen release temperature (~680 °C), after melting at 625 °C [55]. The behaviour of KBH_4 during heating is displayed in Figure 4. The initially white powder is noticeably discoloured above 540 °C, darkening to a yellow/brown tinged powder, indicating that hydrogen release begins in the solid-state in a similar manner to $NaBH_4$. Unexpectedly, the powder takes on a green/blue shade above 590 °C that was difficult to capture by photography. Obvious melting of the powder occurred at 606 °C, below the previously reported melting point. Photography above this temperature was made difficult by the deposition of a thin translucent brown/orange layer on the hot glass as shown in Figure 4. This layer became flakey after cooling and could be a result of a reaction of borohydride vapour with the glass cell at high temperature [24]. After cooling, the consolidated pellet was highly inhomogeneous with noticeably dark blue regions within a white matrix and dark brown/black speckling that may be a separate decomposition product, e.g. a reaction between the KBH_4 and the glass vessel.

A.4. $Mg(BH_4)_2$

The melting behaviour of $Mg(BH_4)_2$ has been contested since the earliest literature [57], but was recently shown to melt at ~280 °C [28]. The diverging reports in the literature appear to be a consequence of the close proximity of the melting point to the decomposition temperature. If there is not sufficient hydrogen backpressure then $Mg(BH_4)_2$ will decompose before melting is observed. Our previous study [28] was performed within a small (8 mL) sealed vessel, allowing hydrogen pressure to inhibit complete decomposition of $Mg(BH_4)_2$ so that melting could be observed. Herein we allow gas to be released during thermal treatment, maintaining a total pressure of ~1 bar system pressure (Ar + H_2) and, as can be seen from Figure 5, no melting behaviour is observed. Other experimental factors may also contribute to the observation (or lack thereof) of melting, such as the thermal ramp rate, atmosphere, and backpressure of hydrogen. The colour changes during decomposition of $Mg(BH_4)_2$ are well known [28] and this sample behaves in a similar manner. The powder is initially white and of very low density before a noticeable reduction in the powder volume occurs between ~150 °C and 175 °C where the γ-$Mg(BH_4)_2$ to ε-$Mg(BH_4)_2$ phase transition is known to occur [28, 58]. In this case there is no observable melting event, but after 280 °C the powder begins to yellow and then darken further to a noticeable brown colour by 400 °C as a result of hydrogen release (Figure 6) and solid-state phase changes in the powder.

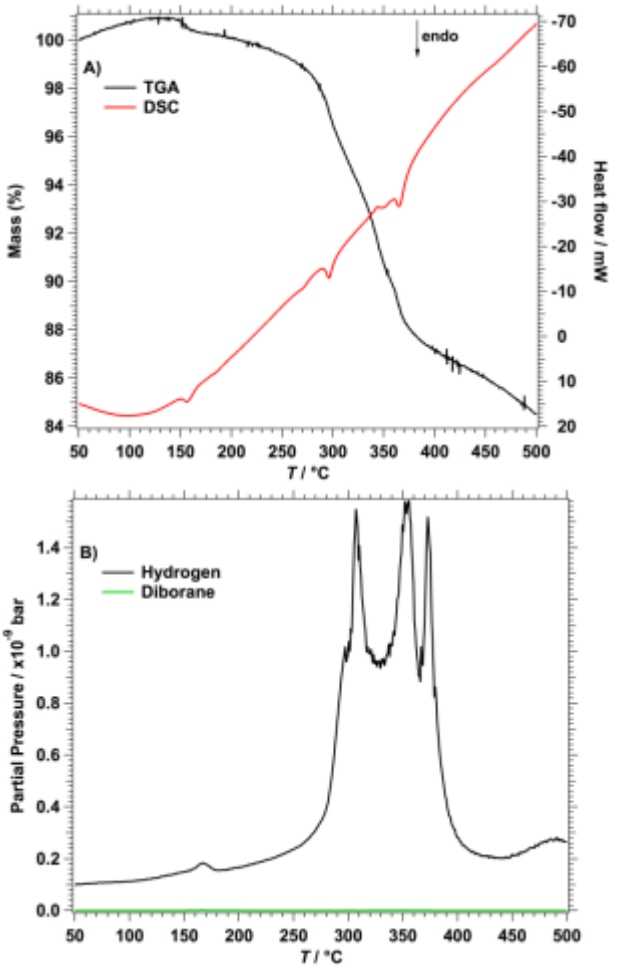

Figure 6: A) TGA, DSC and B) MS data collected simultaneously during the thermolysis of $Mg(BH_4)_2$ under flowing argon.

A.5. $Ca(BH_4)_2$

Recent reports in the literature that $Ca(BH_4)_2$ undergoes solid phase decomposition without melting [59] is in contrast to our findings here. Figure 7 displays the melting of $Ca(BH_4)_2$ above 370 °C, followed by rapid resolidification at higher temperatures (in a similar manner to $Mg(BH_4)_2$ in earlier work [28]), due to decomposition of the melt. It is very likely that the hydrogen backpressure on $Ca(BH_4)_2$ will have an effect on whether the melt exists or not. High hydrogen backpressure will restrict decomposition to higher temperatures and will allow the

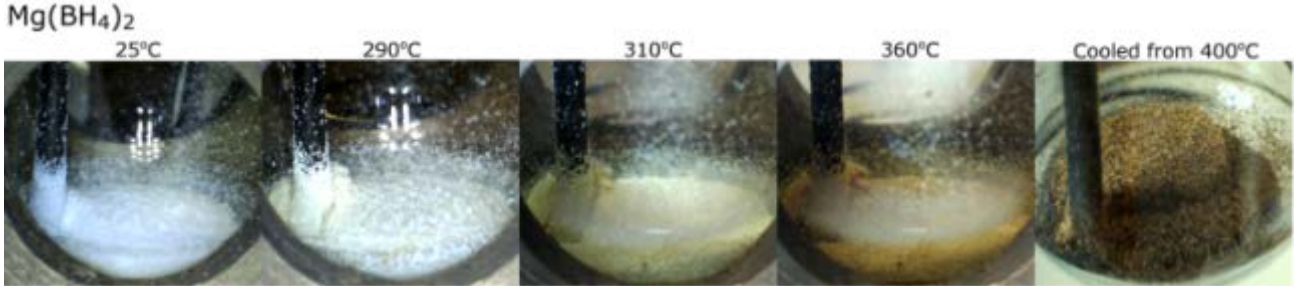

Figure 5: Photographic sequence during thermolysis of $Mg(BH_4)_2$ at 10 °C/minute under argon and evolved gases maintained at 1 bar.

View Article Online
DOI: 10.1039/C3CP53920B
ARTICLE PCCP

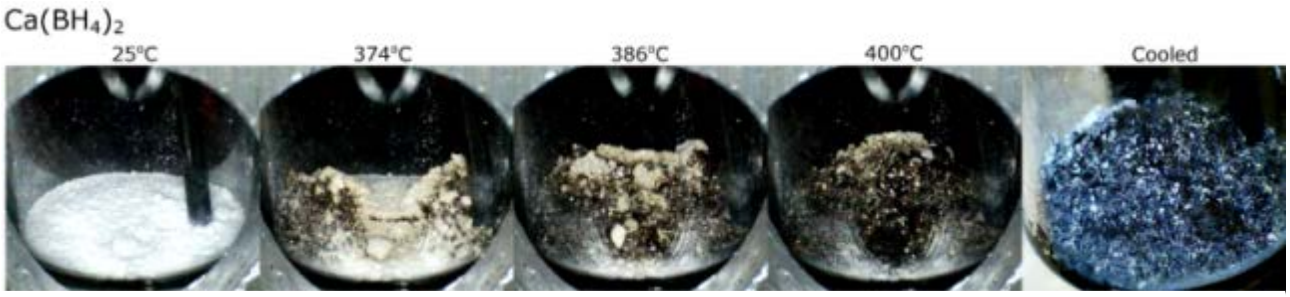

Figure 7: Photographic sequence during thermolysis of $Ca(BH_4)_2$ at 10 °C/minute under argon and evolved gases maintained at 1 bar.

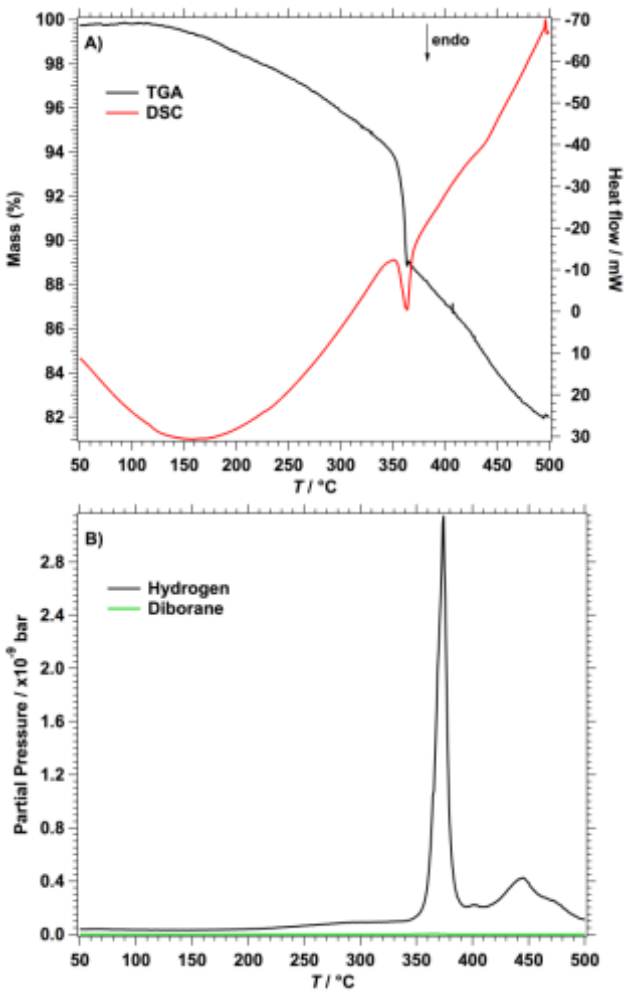

Figure 8: A) TGA, DSC and B) MS data collected simultaneously during the thermolysis of $Ca(BH_4)_2$ under flowing argon.

melting event to be observable. Backpressure has also recently been shown to control the decomposition pathway in this system [30].

A study in 2008 [60] measured a ~6 wt% mass loss from $Ca(BH_4)_2$ near 370 °C coupled by a strong endothermic event and hydrogen gas evolution, in agreement with our visual observations here. This study [60] also resolves a second hydrogen release near 450 °C coupled with an endothermic signature. The thermal decomposition behaviour of $Ca(BH_4)_2$ appears to be affected by the presence of oxygen in a number of studies [61-63] (Further discussion is provided in Section E). The issues with contamination along with minor differences in the decomposition behaviour of different polymorphs of $Ca(BH_4)_2$ [64] cause the analysis of this system to be quite complex. A recent TPD measurement of $Ca(BH_4)_2$ displays significant hydrogen release at 250 and 320 °C, before the pure phase should melt, but very high quantities of CaO are detected in the decomposition products in this study [63]. In our photographic, DSC & MS studies (Figure 8) we do not observe any event near 250 °C, and the $Ca(BH_4)_2$ powder appears white and undisturbed until just before melting is observed at ~370 °C.

A.6. $Mn(BH_4)_2$

$Mn(BH_4)_2$ is reported to melt at ~177 °C [65], although this was mixed with LiCl and no information regarding the backpressure or atmosphere was provided. No endothermic signature is found at this temperature in a later study (under flowing Ar) [66], but a strong endotherm is detected at 150 °C, coupled by an 8.5 wt% mass loss and the evolution of H_2 and B_2H_6. This sample appears to have decomposed before melting could be observed. Samples of $Mn(BH_4)_2$ have also been shown to evolve hydrogen whilst stored at room temperature [67].

The photographic study, Figure 9, conducted for as-synthesized $Mn(BH_4)_2$ did not display obvious melting when

Figure 9: Photographic sequence during thermolysis of $Mn(BH_4)_2$ at 10 °C/minute under argon and evolved gases maintained at 1 bar. Photographs are also shown of a sample heated rapidly at an uncontrolled heat rate using a hot air heat gun.

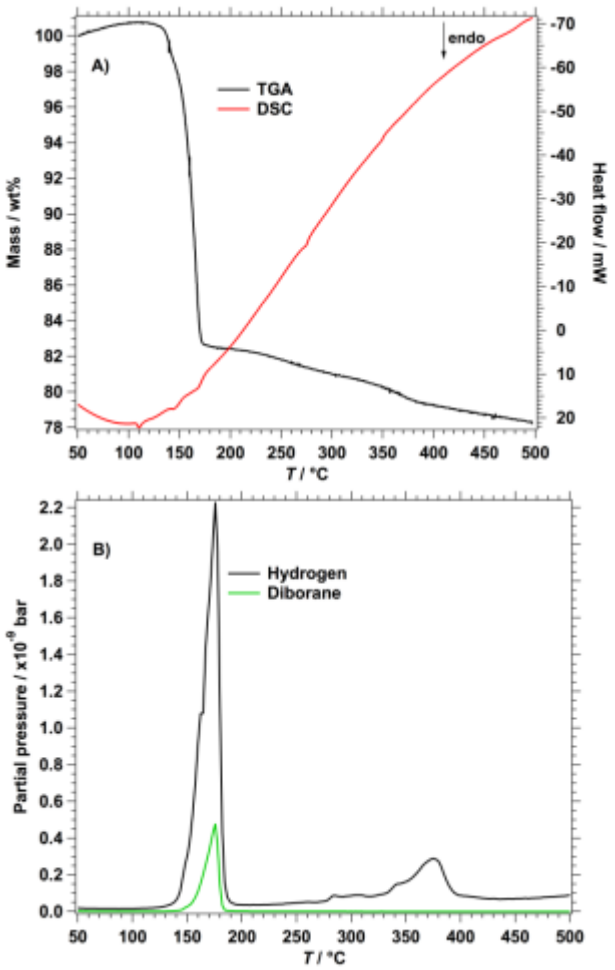

Figure 10: A) TGA, DSC and B) MS data collected simultaneously during the thermolysis of $Mn(BH_4)_2$ under flowing argon.

heated at 10 °C/minute. A colour change from grey to black occurs at ~150 to 160 °C, which coincides with an endothermic peak in the DSC data at ~145 °C (Figure 10). Mass loss from the sample also begins at ~145 °C followed by further major mass loss and gas release occurring from 170 to 180 °C as observed in both TGA and MS data. The major decomposition event coincides with an endothermic peak in the DSC data at ~165 °C. In the photographic study no further changes are observed after the colour change, and the combined study suggests that, with low heating rates, $Mn(BH_4)_2$ decomposes in the solid state without the formation of a molten phase. The $Mn(BH_4)_2$ powder is partially fused after heating, suggesting that $Mn(BH_4)_2$ may begin to melt but decompose at the same time. When $Mn(BH_4)_2$ is heated very rapidly (~10 °C/s) with a heat gun an obvious melting event occurs (see Figure 9). It is likely that rapid heating allows for melting of pure $Mn(BH_4)_2$ to be observed before decomposition products can form. Thus, the $Mn(BH_4)_2$ that was heated slowly is allowed to decompose before reaching its melting point, masking this event by the large quantity of decomposition products present.

Two other endothermic peaks at ~110 and ~273 °C are observed in the DSC data for the $Mn(BH_4)_2$ sample investigated here. These events unfortunately originate from the polymorphic phase change and melting of residual $LiBH_4$ in the sample after the synthesis of $Mn(BH_4)_2$, but this is not observed in X-ray diffraction data (Figure S2). The melting of $LiBH_4$ is not observed in the photographic study, likely due to the fact that only a small amount remains (likely a few percent given the magnitude of the endotherms in the DSC). The total mass loss from RT to 500 °C observed in the TGA data is ~22.4 wt% and the released gas consists of both of H_2 and B_2H_6.

B. $LiBH_4$-$NaBH_4$

Early research into the $LiBH_4$-$NaBH_4$ system in 1961 [68] approximated the eutectic at 224 °C (for 60 mol% $LiBH_4$). However, a revised eutectic was reported at 213 °C (for ~62 mol% $LiBH_4$) in 1971 [69]. This study also determined a large solid solution compositional range between $NaBH_4$ and the high temperature $LiBH_4$ polymorph. Photography, TGA, DSC, and MS data during thermal ramping are provided in Figure 11 and 12 for $0.62LiBH_4$-$0.38NaBH_4$. The polymorphic transition for $LiBH_4$ is evident at ~110 °C by DSC, indicating that at this temperature it is still present as a discrete phase. Eutectic melting is observed (visually and by DSC) at 210 – 220 °C, in agreement with previous reports, and forms a nearly transparent liquid phase with minor bubbling/frothing. The MS data confirms that there is no significant hydrogen evolution near the melting temperature.

Hydrogen evolution becomes apparent above 300 °C from TGA and MS, however only small bubbles are observed in the melt, with no obvious frothing or splattering. Above 350 °C a white film is deposited on the sample cell well above the liquid level that is coupled with hydrogen release. Soon after, there is an obvious vertical spreading of the liquid phase for several centimetres up the walls of the cell that occurs in a matter of seconds. This phenomenon is similar to molten LiH or $LiBH_4$, which are known to creep up the sides of container walls,

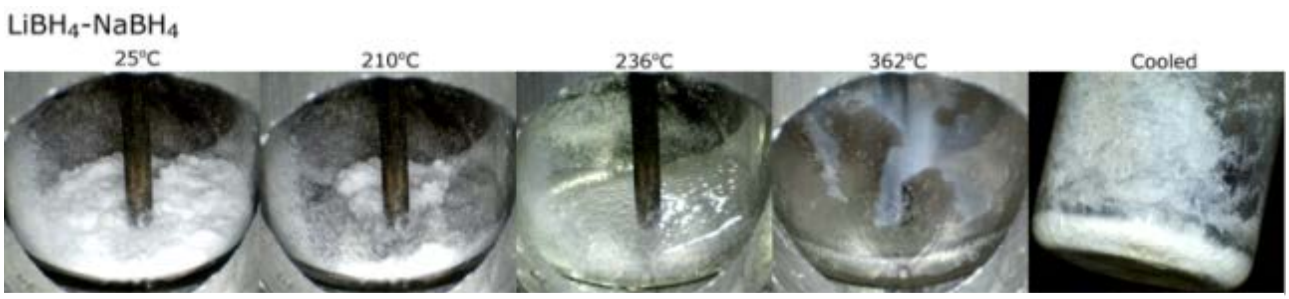

Figure 11: Photographic sequence during thermolysis of $0.62LiBH_4$-$0.38NaBH_4$ at 10 °C/minute under argon and evolved gases maintained at 1 bar.

View Article Online
DOI: 10.1039/C3CP53920B

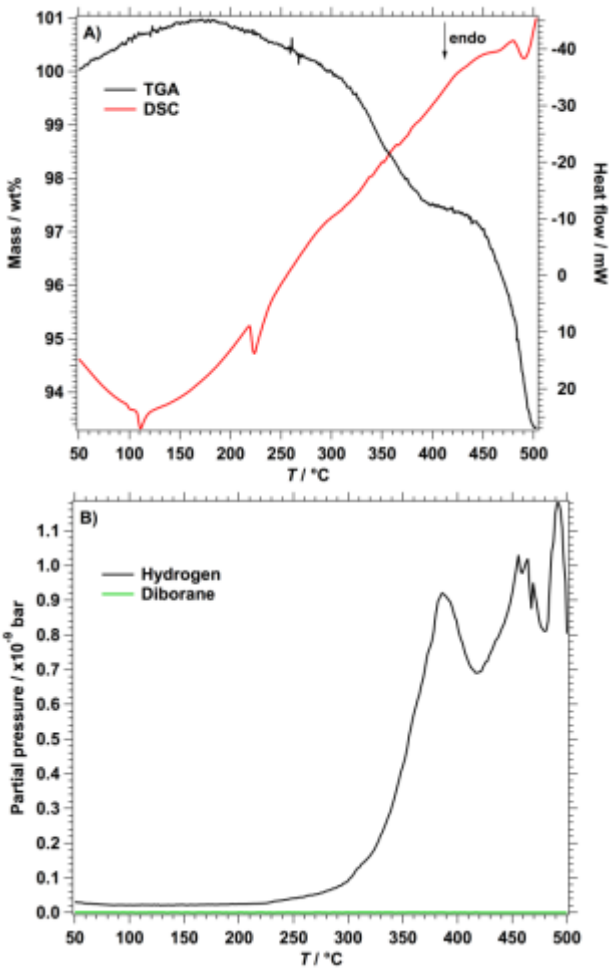

Figure 12: A) TGA, DSC and B) MS data collected simultaneously during the thermolysis of $0.62LiBH_4$-$0.38NaBH_4$ under flowing argon.

depending on temperature, purity, and the wall material [35, 70].

A second hydrogen release event is detected by TGA and MS at 450 °C, followed by a third event close to 500 °C. Some of these hydrogen release events are difficult to discern from DSC due to their very broad signals. It is unexpected to observe 3 decomposition events, when $LiBH_4$ typically only has one event in this temperature range (at ~440 °C [35]) and $NaBH_4$ decomposes at approximately 500 °C. Therefore, the lowest hydrogen release event (385 °C) is surprising and may be due to a destabilizing interaction between both of the cations (Li^+ and Na^+) and the borohydride anions in the liquid phase.

C. $LiBH_4$-KBH_4

A readily fusible eutectic in the $LiBH_4$-KBH_4 system, described in 1961, [68] occurs at 103 °C (for 53 mol% KBH_4). The dual cation salt, $LiK(BH_4)_2$, has since been formed by heating 1:1 mixtures of $LiBH_4$ and KBH_4 for 12 h at 125 °C and is reported to melt at 240 °C [71]. However, this melting point does not agree with the phase diagram [68] and it is expected that a melting point should be closer to the previously reported eutectic temperature (~100 °C). Due to the existence of this dual cation borohydride it is expected that samples of $LiBH_4$-KBH_4 quenched from the molten state will form at least some $LiK(BH_4)_2$.

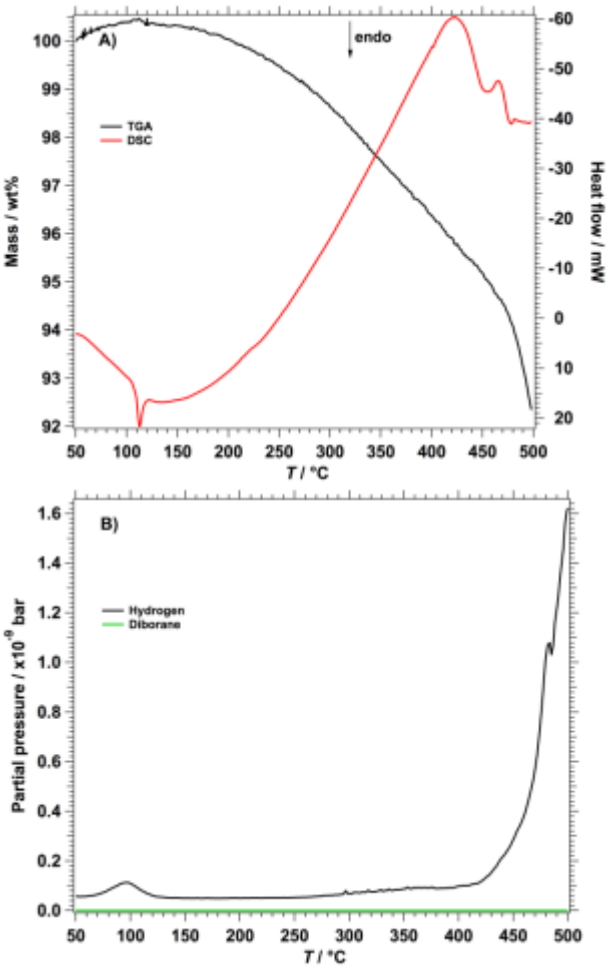

Figure 14: A) TGA, DSC and B) MS data collected simultaneously during the thermolysis of $0.5LiBH_4$-$0.5KBH_4$ under flowing argon.

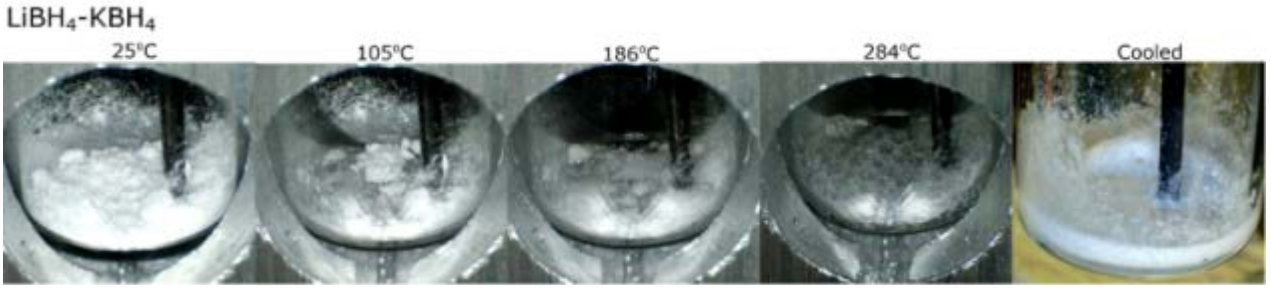

Figure 13: Photographic sequence during thermolysis of $0.5LiBH_4$-$0.5KBH_4$ at 10 °C/minute under argon and evolved gases maintained at 1 bar.

Photography, TGA, DSC, and MS data during thermal ramping are provided in Figure 13 and 14 for $0.5LiBH_4$-$0.5KBH_4$. An obvious melting event is detected just above 100 °C by DSC and photography, where a significant fraction of the sample transitions into a transparent melt. However, there is also a large fraction that appears opaque and solid. It is possible that the 50 mol% composition is just a peritectic point in the phase diagram and is not the true eutectic composition. At 100 °C an increase in the hydrogen signal in the MS data is also observed. This is believed to be associated with the melting of $LiBH_4$ and KBH_4 and reaction with the impurities therein. Interestingly this effect was not observed in the $LiBH_4$-$NaBH_4$ sample and the effect is more likely caused by KBH_4 than $LiBH_4$. Upon heating to 280 °C (the melting point of pure $LiBH_4$) the opaque parts of the sample appear to join the molten phase to form a uniform transparent melt. This suggests that there is excess $LiBH_4$ in the $0.5LiBH_4$-$0.5KBH_4$ composition. In the initial eutectic study [68], the phase diagram was only partially assessed for KBH_4 concentrations < 50 mol%, so the true eutectic point may exist at compositions more rich in KBH_4. However, no DSC event is observed at 280 °C indicating that all the $LiBH_4$ has already melted or has melted over a wide enough temperature range that it is difficult to detect. A small increase in the hydrogen signal in the MS data follows from 300 to 350 °C, before major release starts at 450 °C, slightly above the decomposition temperature of pure $LiBH_4$. The decomposition is accompanied by a large signal in the DSC and MS curves.

D. $LiBH_4$-$Mg(BH_4)_2$

Eutectic behaviour in the $LiBH_4$-$Mg(BH_4)_2$ system was noted in 2011 [72] where a eutectic melt was suggested to occur below 183 °C for compositions rich in $Mg(BH_4)_2$. In the same year, a more comprehensive study of the $LiBH_4$-$Mg(BH_4)_2$ system was undertaken [73] where a eutectic was found at 180 °C for a composition between 50 - 60 mol% $LiBH_4$. It should be noted that an earlier study in 2010 [74] reported the existence of "$Li_{1-x}Mg_{1-y}(BH_4)_{3-x-2y}$" that appears to be misassigned from an XRD pattern of what is actually α-$Mg(BH_4)_2$. Later studies [73] verify the existence of physical mixtures of $LiBH_4$ and $Mg(BH_4)_2$ rather than a dual cation phase.

Photography, TGA, DSC, and MS data during thermal ramping are provided in Figure 15 and 16 for $0.55LiBH_4$-$0.45Mg(BH_4)_2$. The polymorphic transition for $LiBH_4$ is evident at ~105 °C by DSC, indicating that at this temperature it is still present as a discrete phase. There is an endothermic event detected at 170 °C that is coupled by a minor hydrogen release. This event has been previously assigned to eutectic melting, overlapping with the α to β $Mg(BH_4)_2$ phase transition [75]. Unexpectedly, the powder does not obviously melt at this temperature (see Figure 15), and still retains a powder-like form above 190 °C. The lack of an obvious molten phase may be an issue for nanoconfinement studies. A $0.5LiBH_4$-$0.5Mg(BH_4)_2$ composition has previously been heated to 190 °C [75] under 40 bar H_2 for 1 hour to 'melt impregnate' an activated carbon.

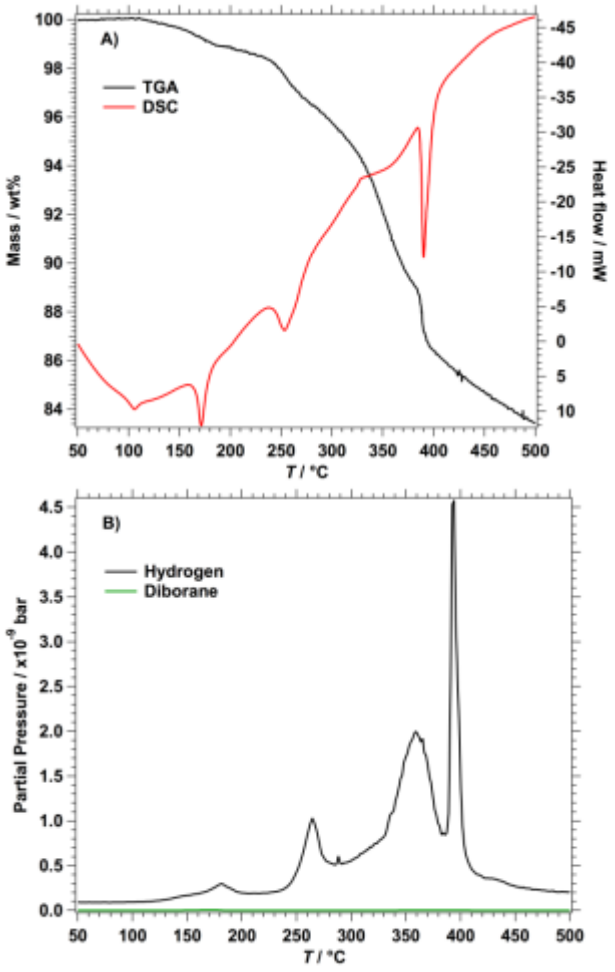

Figure 16: A) TGA, DSC and B) MS data collected simultaneously during the thermolysis of $0.55LiBH_4$-$0.45Mg(BH_4)_2$ under flowing argon.

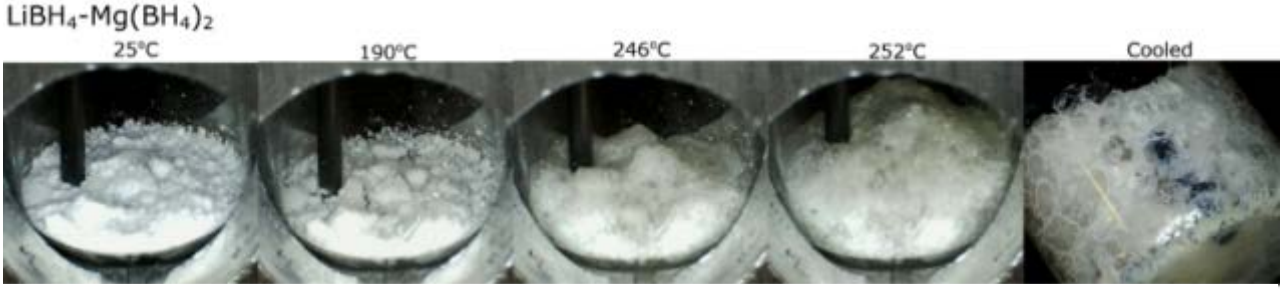

Figure 15: Photographic sequence during thermolysis of $0.55LiBH_4$-$0.45Mg(BH_4)_2$ at 10 °C/minute under argon and evolved gases maintained at 1 bar.

View Article Online
DOI: 10.1039/C3CP53920B

Unfortunately the $LiBH_4$-$Mg(BH_4)_2$ composite in Figure 15 does not appear conducive to melt infiltration at 190 °C or even by 250 °C as it is not a distinctive liquid phase. It is possible that the hydrogen overpressure and the isothermal wait time would allow a proper liquid eutectic to form, allowing nanoconfinement to be possible. The DSC and NMR data after 'nanoconfinement' [75] do suggest that changes in the borohydrides have occurred, assigned to the fact that they are nanoconfined. The endothermic event at 170 °C has also previously been linked to diborane evolution [73] but appears to be related to impurities as we only observe a small hydrogen release peak and not diborane.

There is notable hydrogen release above 250 °C from MS that is linked to severe sample frothing by photography and an endothermic spike in DSC. This hydrogen release is seen in other studies [73] and is very interesting because neither of the borohydrides, in their pure form, release hydrogen at this temperature. It is likely that this is made possible by the fact that they are now molten. $LiBH_4$ normally melts at 280 °C, releasing hydrogen above 330 °C, and $Mg(BH_4)_2$ also normally melts at 280 °C, but releases hydrogen immediately upon melting. The hydrogen event at 360 °C appears to be related to the release from $Mg(BH_4)_2$, whilst the 400 °C event is likely from $LiBH_4$. However the position and shape of these events has changed when compared to the pure systems implying that there may be a different kinetic and/or thermodynamic mechanism for hydrogen release in the eutectic system.

E. $LiBH_4$-$Ca(BH_4)_2$

The $LiBH_4$-$Ca(BH_4)_2$ system was investigated in 2009 [76] where a eutectic composition was located between 60 – 80 mol% $LiBH_4$ that melted at ~200 °C. The eutectic composition was more accurately determined to be $0.68LiBH_4$-$0.32Ca(BH_4)_2$ in 2011 [61] from DSC studies of different molar ratios. A mixture of $0.7LiBH_4$-$0.3Ca(BH_4)_2$ was heated from room temperature to 400 °C as shown in Figure 17 and 18. The endothermic events observed by DSC are similar to those detected by Lee *et al.* [61]. From this DSC data the polymorphic transition for $LiBH_4$ is evident at ~110 °C, followed by polymorphic transitions for $Ca(BH_4)_2$ at ~140 °C [76] and an eutectic melting event at ~200 °C. There is noticeable bubbling of the eutectic at 250 °C (with no precursor liquid phase), where the solid powder appears to swell up into the froth shown in Figure 17. The bubbling is not coupled by any major endothermic spike or major H_2 release. However other studies [61, 62] have found that, at this temperature, $Ca_3(BH_4)_3(BO_3)$ can form from as-yet undetermined means. It

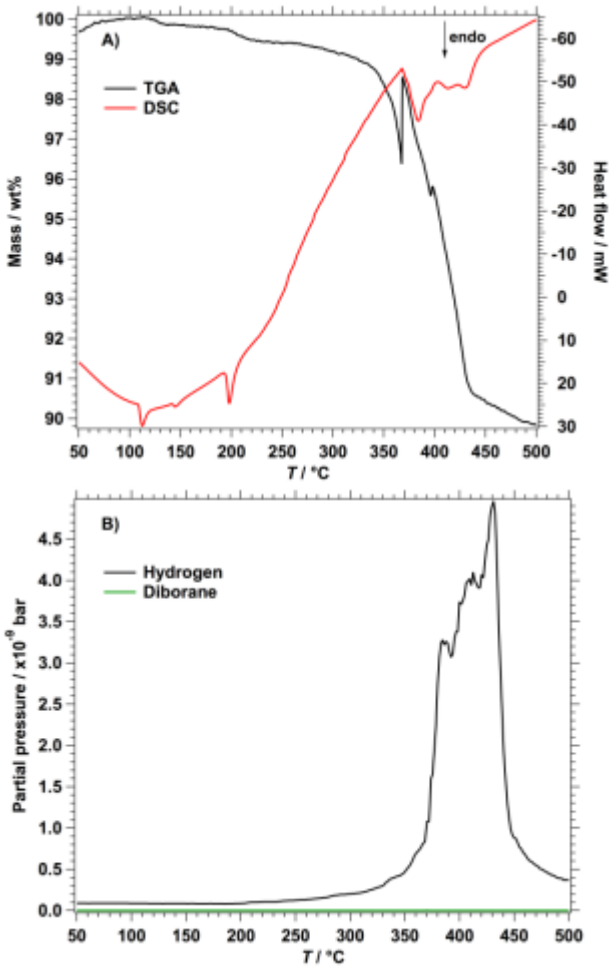

Figure 18: A) TGA, DSC and B) MS data collected simultaneously during the thermolysis of $0.7LiBH_4$-$0.3Ca(BH_4)_2$ under flowing argon.

is possible that the oxygen is located in the starting reagents, possibly from residual adducts [77], adsorbed water, an air leak, or even in some cases, glass (SiO_2).

There is a major H_2 release above 350 °C as shown by TGA and MS, consistent with earlier studies [76]. There is also a strong artefactual spike in the TGA at this point, associated with the bubbling observed by photography, that is more pronounced in an earlier study over 250 – 350 °C [78]. In fact, this earlier study detected the formation of a new phase by XRD after ball milling that was thought to be a dual cation $LiCa(BH_4)_3$ phase. Although this is as-yet unconfirmed, it may be a result of the very high levels of CaO observed after heating, especially given

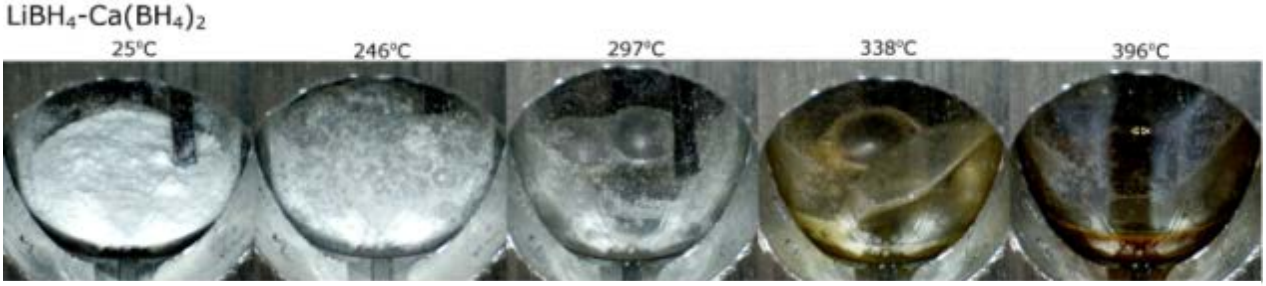

Figure 17: Photographic sequence during thermolysis of $0.7LiBH_4$-$0.3Ca(BH_4)_2$ at 10 °C/minute under argon and evolved gases maintained at 1 bar.

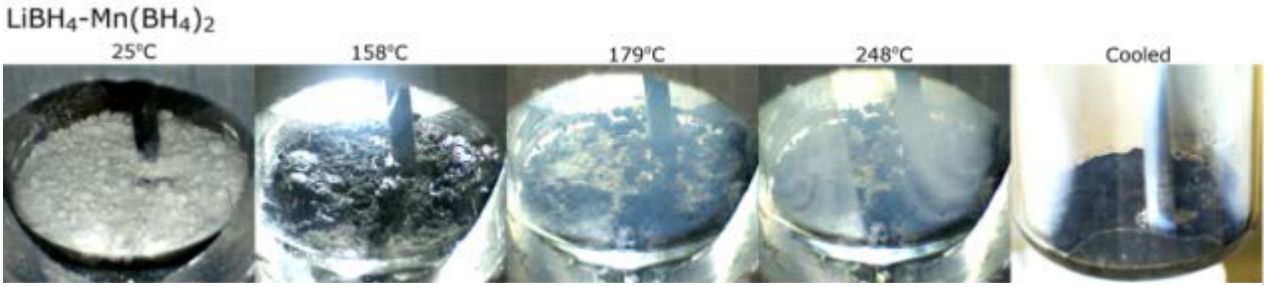

Figure 19: Photographic sequence during thermolysis of 0.5$LiBH_4$-0.5$Mn(BH_4)_2$ at 10 °C/minute under argon and evolved gases maintained at 1 bar.

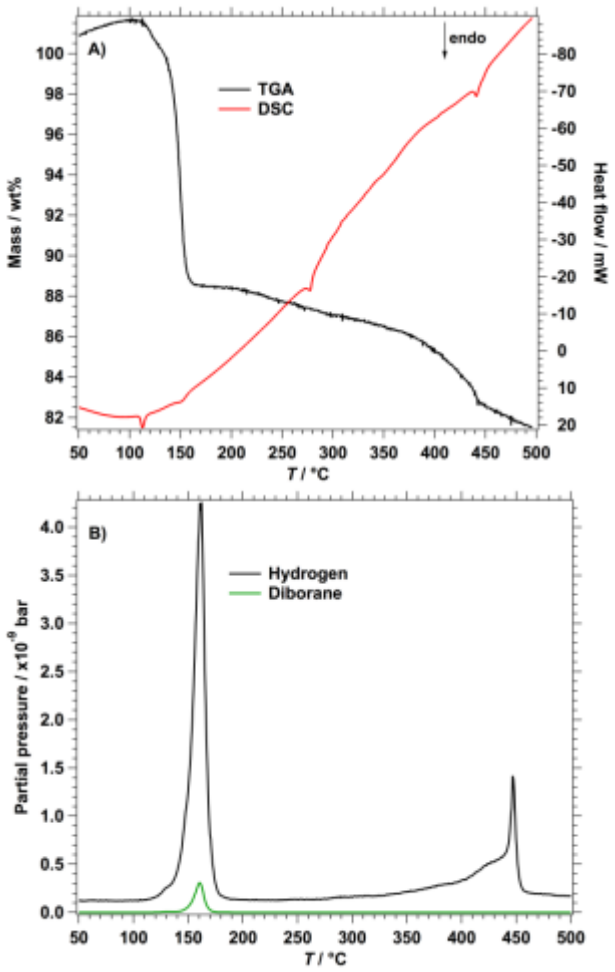

Figure 20: A) TGA, DSC and B) MS data collected simultaneously during the thermolysis of 0.5$LiBH_4$-0.5$Mn(BH_4)_2$ under flowing argon.

that another unknown 'intermediate-II' phase was later identified as $LiCa(BH_4)(BO_3)_2$ [79]. However, a recent in-situ NMR study [80] does indicate the formation of a mixed cation (Li/Ca) borohydride at 100 – 170 °C, presumed to be facilitated by a carbon scaffold, acting to promote the exchange of cations in the solid-state. Despite promising results in this study, these nanoconfined samples are also affected by oxygen with the generation of substantial levels of $Ca_3(BH_4)_3(BO_3)$ and $LiCa(BH_4)(BO_3)_2$ after heating.

F. $LiBH_4$-$Mn(BH_4)_2$

The $LiBH_4$-$Mn(BH_4)_2$ system has not been explicitly studied to date. However, a recent study [66] has performed analyses on $Mn(BH_4)_2$ mechanochemically synthesized from 3$LiBH_4$ + $MnCl_2$ (i.e. $Mn(BH_4)_2$ with LiCl and excess $LiBH_4$). This is essentially a ternary 0.2$LiBH_4$-0.4$Mn(BH_4)_2$-0.4LiCl system. A lowered hydrogen release temperature is detected for this system (130 °C) in comparison to the 0.5$Mn(BH_4)_2$-0.5LiCl system (148 °C). This lowered decomposition event may be due to a lower temperature eutectic melting liquid phase transition: a possibility supported by *in-situ* XRD data that showed the loss of crystalline peaks at a lower temperature [66]. Our MS data (on LiCl-free samples) also supports the notion of eutectic melting, where hydrogen desorption from 0.5$LiBH_4$-0.5$Mn(BH_4)_2$ occurs ~20 °C lower than for $Mn(BH_4)_2$ (see Figure 10 and 20).

The photographs collected during thermal ramping are displayed in Figure 19. The slightly off-white powder turns near-black at ~150 °C in the solid state. This colour transition is then followed by a liquification wave that quickly runs through the sample just before reaching 160 °C. The solid-liquid phase change is coupled by a significant mass loss (~12 %) and the evolution of both hydrogen and diborane. At higher temperature the cooler parts of the glass are steadily coated by an opaque white layer. High temperature hydrogen release at > 350 °C is also observed, which is consistent with $LiBH_4$ decomposition. Cooling reveals a pellet that is no longer well-powdered, having transitioned through a molten phase, that is in contrast to the steady heating of single-phase $Mn(BH_4)_2$.

G. $NaBH_4$-KBH_4

An eutectic was observed in the $NaBH_4$-KBH_4 at 453 °C (for 31.8 mol% KBH_4) in 1971 [69] where the existence of solid solutions is also reported. The existence of room temperature metastable $NaK(BH_4)_2$ has also been reported and was found to transform back into the constituent borohydride phases over the course of hours [81]. The XRD pattern for $NaK(BH_4)_2$ appears to be a compressed cubic KBH_4 or expanded cubic $NaBH_4$ cell and may actually be a solid solution. Photography, TGA, DSC, and MS collected during the thermal treatment of a 0.68$NaBH_4$-0.32KBH_4 composition is displayed in Figure 21 and 22. A melting event is visually observed at 440 °C, lower than the previously reported temperature (by 13 °C), where the white

View Article Online
DOI: 10.1039/C3CP53920B
ARTICLE PCCP

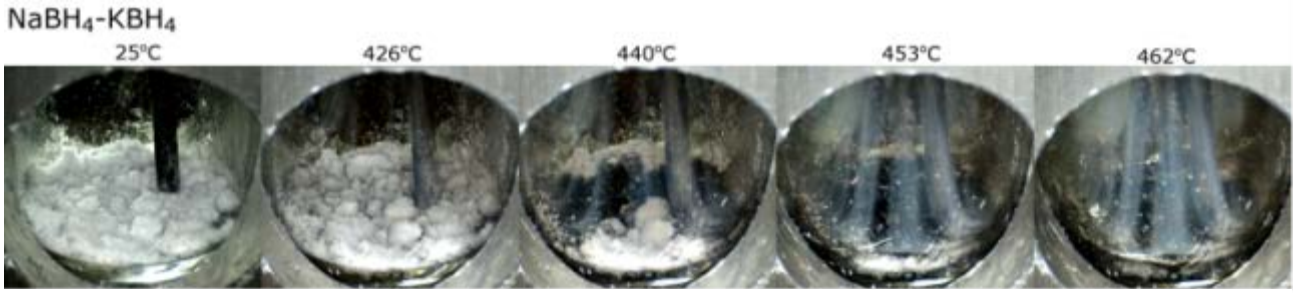

Figure 21: Photographic sequence during thermolysis of 0.68$NaBH_4$-0.32KBH_4 at 10 °C/minute under argon and evolved gases maintained at 1 bar.

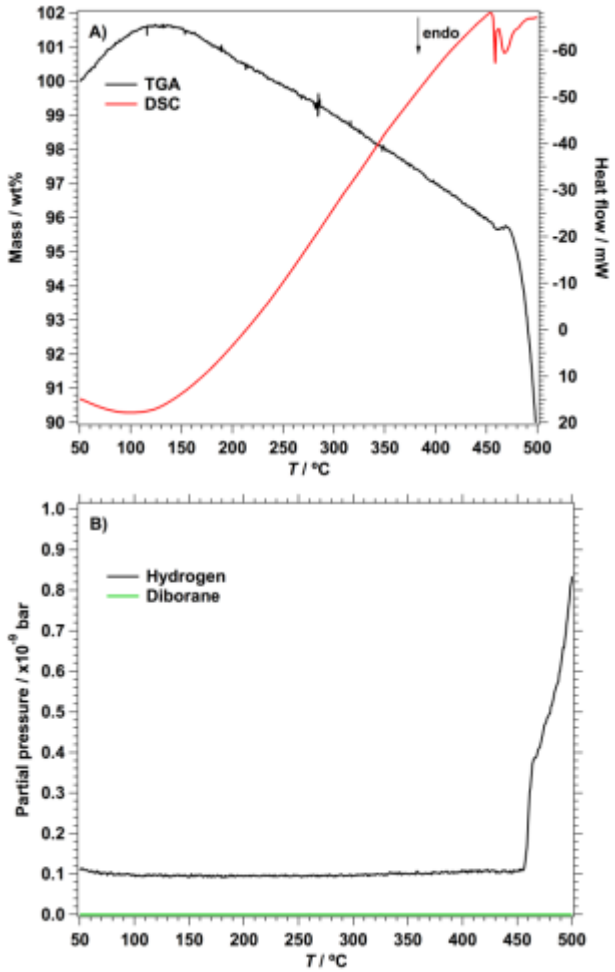

Figure 22: A) TGA, DSC and B) MS data collected simultaneously during the thermolysis of 0.68$NaBH_4$-0.32KBH_4 under flowing argon.

powder transforms into a dark coloured liquid. The melting event is closely followed by a significant hydrogen release near 450 °C, coupled by the deposition of an opaque white film on the surface of the glass. The melting and decomposition is also observed in the DSC data by two endothermic peaks at 450 and 470 °C. Again, the full mass loss is not realized below 500 °C.

H. $LiBH_4$-$NaBH_4$-KBH_4

In 1960 the ternary eutectic of $LiBH_4$-$NaBH_4$-KBH_4 was reported to be at 96 °C with a composition 0.45$LiBH_4$-0.1$NaBH_4$-0.45KBH_4 [82]. Photography, TGA, DSC, and MS data collected during thermal ramping for this composition are provided in Figure 23 and 24. An endothermic peak is observed in the DSC data at 108 °C that originates from a melting event. In the similar 0.5$LiBH_4$-0.5KBH_4 system, the endothermic melting event is found at 113 °C. Pure $LiBH_4$ also has a polymorphic transition at this temperature. In the photo experiment in Figure 23 the sample visually begins to melt at 103 °C rather than 96 °C. It appears as though there is a small difference in the melting point of the ternary sample compared to the similar binary system (that does not have $NaBH_4$). However, this difference is not as large as noted in the original study on 0.45$LiBH_4$-0.1$NaBH_4$-0.45KBH_4. In addition, like the binary $LiBH_4$-KBH_4 system, there is only a partial molten transition near 100 °C, whilst the remaining portion of the sample melts at approximately 280 °C. This indicates that this composition is $LiBH_4$-rich and not a perfect eutectic mixture.

I. Comparisons

Most of the borohydrides and their mixtures tend to behave in a varied manner to one another with regards to melting. It is likely that these differences are a function of multiple factors

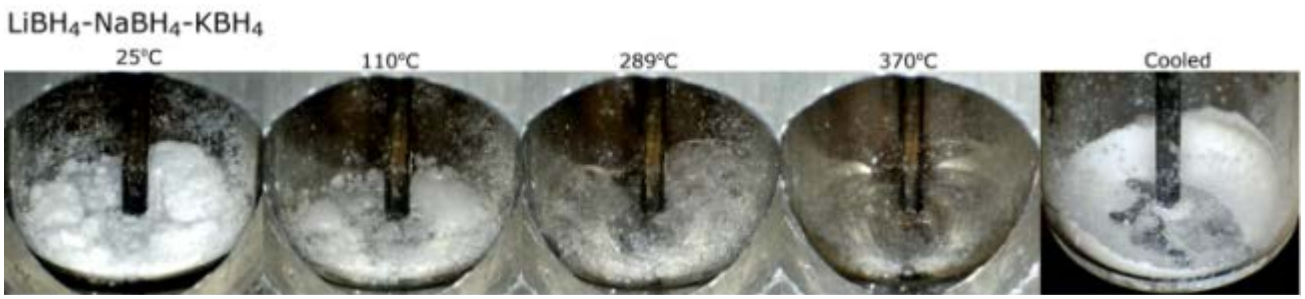

Figure 23: Photographic sequence during thermolysis of 0.45$LiBH_4$-0.1$NaBH_4$-0.45KBH_4 at 10 °C/minute under argon and evolved gases maintained at 1 bar.

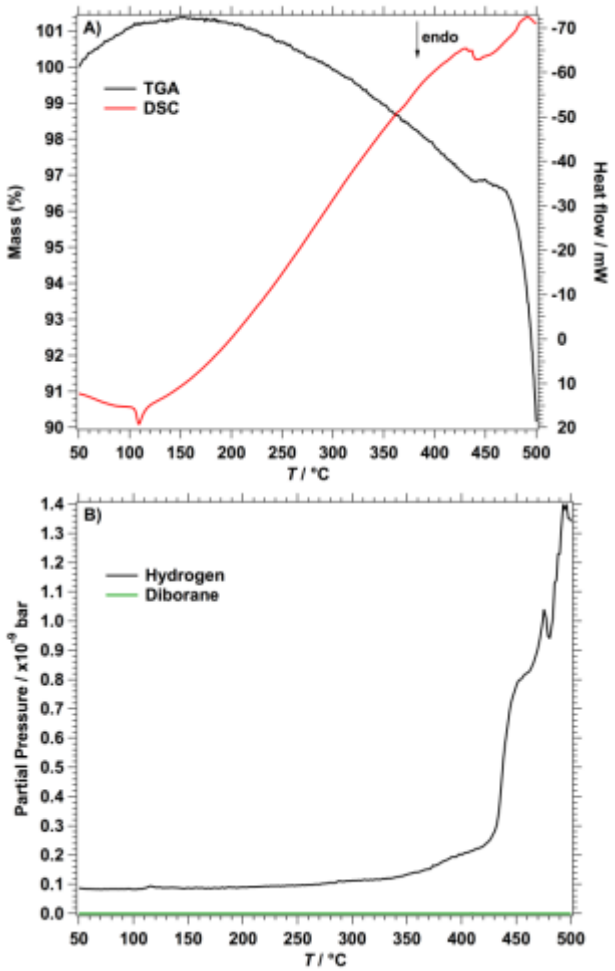

Figure 24: A) TGA, DSC and B) MS data collected simultaneously during the thermolysis of $0.45LiBH_4$-$0.1NaBH_4$-$0.45KBH_4$ under flowing argon.

such as viscosity, surface tension, the vicinity of decomposition temperature to the melting point, and even the nature of the decomposition products. The decomposition products after heating appeared different in most cases and largely depended on the degree of decomposition achieved in each system. None of the systems displayed any metallic decomposition products on visual inspection, suggesting that after heating the products were likely the precursor borohydrides, higher metal boranes, metal hydrides, or metal borides. Given the complexity of each system, studies need to be undertaken on individual systems with a comprehensive suite of analytical techniques. Impurities are also a large concern with the analysis of borohydrides and some cases, such as $Ca(BH_4)_2$, appear worse than others. The impurities can cause unwanted alterations to the decomposition pathways and can have a significant influence on the bubbling and frothing during melting, even in minor quantities (i.e. only causing minor H_2 evolution). In this study the total pressure was kept constant at 1 bar, but the partial pressure of hydrogen may increase prior to melting in cases where hydrogen is released from the sample. The gas composition and total pressure may alter the dehydrogenation reaction by kinetically suppressing the formation of the diborane by-product [83]. The

Table 1: Summary of the melting and decomposition behavior for metal borohydrides and mixtures.

System	*Event Temperature (°C)*	*Nature*
$LiBH_4$	110	Polymorphic transition
	280	Melting (transparent liquid)
	> 400	Hydrogen release
$NaBH_4$	460	Color change (hydrogen release)
	510	Melting (transparent liquid)
KBH_4	540	Color change (hydrogen release)
	605	Melting
γ-$Mg(BH_4)_2$	160	Polymorphic transition
	280	Color change (hydrogen release)
	350	Hydrogen release
	370	Hydrogen release
$Ca(BH_4)_2$	370	Melting (hydrogen release)
	440	Hydrogen release
$Mn(BH_4)_2$	145	Hydrogen & diborane release
	170	Hydrogen & diborane release
$0.62LiBH_4$-$0.38NaBH_4$	110	$LiBH_4$ polymorphic transition
	215	Melting (transparent liquid)
	> 300	Hydrogen release
	460	Hydrogen release
	490	Hydrogen release
$0.5LiBH_4$-$0.5KBH_4$	110	Melting (partial)
	280	Melting (complete)
	> 420	Hydrogen release
$0.55LiBH_4$-$0.45Mg(BH_4)_2$	105	$LiBH_4$ polymorphic transition
	170	Hydrogen release (minor)
	250	Hydrogen release (frothing)
	360	Hydrogen release
	390	Hydrogen release
$0.7LiBH_4$-$0.3Ca(BH_4)_2$	110	$LiBH_4$ polymorphic transition
	200	Thermal signature with no obvious melting
	250	Frothing/expansion
	> 300	Bubbling (large bubbles)
	> 350	Hydrogen release
$0.5LiBH_4$-$0.5Mn(BH_4)_2$	110	$LiBH_4$ polymorphic transition
	150/160	Melting (partial)
	150/160	Hydrogen & diborane release
	280	Thermal signature (possible $LiBH_4$ melting)
	> 350	Hydrogen release
$0.68NaBH_4$-$0.32KBH_4$	440	Melting (dark colored liquid)
	> 450	Hydrogen release
$0.45LiBH_4$-$0.1NaBH_4$-$0.45KBH_4$	110	Melting (partial)
	280	Melting (complete)
	> 400	Hydrogen release

hydrogen backpressure has a definite effect in controlling the decomposition temperature for all of the borohydrides and their mixtures. Under low hydrogen backpressure some borohydrides can decompose in the solid-state before melting is observed. In addition, the effect of gas pressure on the formation and persistence of froth and/or bubbling in the borohydride systems is not yet fully known.

All the monometallic borohydrides decompose closely before or after their respective melting points (Table 1). The formation of a eutectic mixture can allow for earlier decomposition at lower temperatures during thermal ramping. It is not yet known if this is enabled by a thermodynamic or kinetic enhancement. The structural reorganization upon

View Article Online
DOI: 10.1039/C3CP53920B
ARTICLE PCCP

melting [80] may in fact result in different bonding energies and therefore enable hydrogen release from certain borohydrides upon melting. This phenomenon may also allow for rehydrogenation at lower temperatures for eutectic systems due to energy differences in the ionic borohydride melt at lower temperatures.

Conclusions

Understanding the melting, bubbling and frothing of borohydrides and their mixtures is of great importance to their implementation into technological applications, i.e. a solution is more conveniently handled as compared to a solid. High temperature solid-liquid phase changes may be desirable in some applications, such as solar thermal energy storage [5], but are undesirable from a hydrogen storage standpoint. This is because, at present, the transformation of a powder into a liquid completely destroys any microstructure, dramatically reduces the surface area, redistributes any catalysts and causes significant reversibility issues.

It would be interesting to conduct further experiments under a series of hydrogen and inert gas backpressures to elucidate the impact backpressure has on the physical properties of the borohydrides upon melting. It is clear that the physical phenomena of uncontrolled bubbling and frothing could be detrimental to the use of borohydrides in technological applications. This study reveals that visual inspection of bulk materials during thermolysis can be very informative, in particular when used in combination with analysis of mass loss and evolved gas composition. This technique may be useful for the characterization of a range of other materials which evolve a gas during thermolysis.

Acknowledgements

CEB, MP & DAS acknowledge the financial support of the Australian Research Council for ARC Linkage Grant LP120100435. The work was supported by the Danish National Research Foundation, Center for Materials Crystallography (DNRF93), the Danish Strategic Research Council (the research project HyFillFast), and by the Danish Research Council for Nature and Universe (Danscatt). We are grateful to the Carlsberg Foundation.

Notes and references

[a] Department of Imaging and Applied Physics, Fuels and Energy Technology Institute, Curtin University, GPO Box U1987, Perth, 6845 WA, Australia

[b] Interdisciplinary Nanoscience Center (iNANO) and Department of Chemistry, University of Aarhus, DK-800, Denmark

Electronic Supplementary Information (ESI) available: Phase diagrams and physical data for relevant compounds. See DOI: 10.1039/b000000x/

1. M. Faraday, *Experimental Researches in Electricity, Volume I*, Richard and John Edward Taylor, London, 1849.
2. W. Sundermeyer, *Angew. Chem. Int. Ed.*, 1965, **4**, 222-238.
3. G. E. Blomgren and E. R. Van Artsdalen, *Ann. Rev. Phys. Chem.*, 1960, **11**, 273-306.
4. F. Habashi, *Handbook of Extractive Metallurgy, Volume 2*, WILEY-VCH, Heidelberg, Germany, 1997.
5. D. N. Harries, M. Paskevicius, D. A. Sheppard, T. Price and C. E. Buckley, *P. IEEE*, 2012, **100**, 539-549.
6. L. H. Rude, T. K. Nielsen, D. B. Ravnsbæk, U. Bösenberg, M. B. Ley, B. Richter, L. M. Arnbjerg, M. Dornheim, Y. Filinchuk, F. Besenbacher and T. R. Jensen, *Phys. Stat. Sol. A*, 2011, **208**, 1754-1773.
7. T. K. Nielsen, F. Besenbacher and T. R. Jensen, *Nanoscale*, 2011, **3**, 2086-2098.
8. A. K. Galwey, *J. Therm. Anal. Cal.*, 2005, **82**, 23-40.
9. A. K. Galwey, *J. Therm. Anal. Cal.*, 2005, **82**, 423-437.
10. C. E. Johnson and E. J. Hathaway, *J. Chem. Eng. Data*, 1969, **14**, 174-175.
11. P. Ehrlich and W. Deissmann, *Naturwissenschaften*, 1964, **51**, 135.
12. C. E. Johnson, S. E. Wood and C. E. Crouthamel, *Journal of Chemical Physics*, 1966, **44**, 880-883.
13. C. E. Messer and J. Mellor, *J. Phys. Chem.*, 1960, **64**, 503-505.
14. V. I. Mikheeva and S. V. Zapolskii, *Dokl. Akad. Nauk SSSR*, 1966, **171**, 872-873.
15. S. V. Zapolskii, V. M. Bakulina and V. I. Mikheeva, *Zhurn. Neorg. Khim.*, 1967, **12**, 1310-1315.
16. R. Černý, D. B. Ravnsbæk, G. Severa, Y. Filinchuk, V. D' Anna, H. Hagemann, D. r. Haase, J. Skibsted, C. M. Jensen and T. R. Jensen, *J. Phys. Chem. C*, 2010, **114**, 19540-19549.
17. P. Schouwink, V. D'Anna, M. B. Ley, L. M. Lawson Daku, B. Richter, T. R. Jensen, H. Hagemann and R. Černý, *J. Phys. Chem. C*, 2012, **116**, 10829-10840.
18. D. B. Ravnsbæk, Y. Filinchuk, Y. Cerenius, H. J. Jakobsen, F. Besenbacher, J. Skibsted and T. R. Jensen, *Angew. Chem. Int. Ed.*, 2009, **48**, 6659-6663.
19. D. B. Ravnsbæk, L. H. Sørensen, Y. Filinchuk, D. Reed, D. Book, H. J. Jakobsen, F. Besenbacher, J. Skibsted and T. R. Jensen, *Euro. J. Inorg. Chem.*, 2010, **11**, 1608-1612.
20. M. B. Ley, S. Boulineau, R. Janot, Y. Filinchuk and T. R. Jensen, *J. Phys. Chem. C*, 2012, **116**, 21267-21276.
21. M. B. Ley, D. B. Ravnsbæk, Y. Filinchuk, Y.-S. Lee, R. Janot, Y. W. Cho, J. Skibsted and T. R. Jensen, *Chem. Mater.*, 2012, **24**, 1654-1663.
22. C. Frommen, M. H. Sørby, P. Ravindran, P. Vajeeston, H. Fjellvag and B. C. Hauback, *J. Phys. Chem. C*, 2011, **115**, 23591-23602.
23. D. B. Ravnsbæk, M. B. Ley, Y.-S. Lee, H. Hagemann, V. D'Anna, Y. W. Cho, Y. Filinchuk and T. R. Jensen, *Int. J. Hydrogen Energy*, 2012, **37**, 8428-8438.
24. L. Mosegaard, B. Moller, J.-E. Jorgensen, Y. Filinchuk, Y. Cerenius, J. C. Hanson, E. Dimasi, F. Besenbacher and T. R. Jensen, *J. Phys. Chem. C*, 2008, **112**, 1299-1303.
25. L. M. Arnbjerg, D. B. Ravnsbæk, Y. Filinchuk, R. T. Vang, Y. Cerenius, F. Besenbacher, J.-E. Jørgensen, H. J. Jakobsen and T. R. Jensen, *Chem. Mater.*, 2009, **21**, 5772-5782.
26. L. H. Rude, E. Groppo, L. M. Arnbjerg, D. B. Ravnsbæk, R. A. Malmkjær, Y. Filinchuk, M. Baricco, F. Besenbacher and T. R. Jensen, *J. Alloys Compd.*, 2011, **509**, 8299-8305.

27. L. H. Rude, O. Zavorotynska, L. M. Arnbjerg, D. B. Ravnsbæk, R. A. Malmkjær, H. Grove, B. C. Hauback, M. Baricco, Y. Filinchuk, F. Besenbacher and T. R. Jensen, *Int. J. Hydrogen Energy*, 2011, **36**, 15664-15672.
28. M. Paskevicius, M. P. Pitt, C. J. Webb, D. A. Sheppard, U. Filsø, E. M. Gray and C. E. Buckley, *J. Phys. Chem. C*, 2012, **116**, 15231-15240.
29. Y. Zhang, E. Majzoub, V. Ozoliņš and C. Wolverton, *J. Phys. Chem. C*, 2012, **116**, 10522-10528.
30. Y. Kim, S.-J. Hwang, Y.-S. Lee, J.-Y. Suh, H. N. Han and Y. W. Cho, *J. Phys. Chem. C*, 2012, **116**, 25715-25720.
31. D. S. Stasinevich, G. A. Egorenko and G. N. Gnedina, *Dokl. Akad. Nauk SSSR*, 1966, **168**, 610-612.
32. A. Remhof, A. Borgschulte, O. Friedrichs, P. Mauron, Y. Yan and A. Züttel, *Scripta Mater.*, 2012, **66**, 280-283.
33. O. Friedrichs, A. Borgschulte, S. Kato, F. Buchter, R. Gremaud, A. Remhof and A. Züttel, *Chem. Euro. J.*, 2009, **15**, 5531-5534.
34. O. Friedrichs, A. Remhof, S. J. Hwang and A. Züttel, *Chem. Mater.*, 2010, **22**, 3265-3268.
35. M. P. Pitt, M. Paskevicius, D. H. Brown, D. A. Sheppard and C. E. Buckley, *J. Am. Chem. Soc.*, 2013, **135**, 6930-6941.
36. H. Toyoda, M. Watanabe and H. Sugai, *J. Nuc. Mater.*, 1997, **241-243**, 1031-1035.
37. M. Au, A. R. Jurgensen, W. A. Spencer, D. L. Anton, F. E. Pinkerton, S.-J. Hwang, C. Kim and R. C. Bowman, *J. Phys. Chem. C*, 2008, **112**, 18661-18671.
38. M. F. Ashby, A. G. Evans, N. A. Fleck, L. J. Gibson, J. W. Hutchinson and H. N. G. Wadley, *Metal Foams: A Design Guide*, Butterworth Heinemann, Boston, USA, 2000.
39. J. O. M. Bockris, A. Calandra and C. Solomons, *NASA Report*, 1969, **66519A**.
40. A. N. Smith, in *Molten Salt Reactor Program - Semiannual Progress Report*, ed. L. E. McNeese, Oak Ridge National Laboratory ORNL-5047, 1975.
41. G. J. Janz, C. B. Allen, N. P. Bansal, R. M. Murphy and R. P. T. Tomkins, *National Bureau of Standards*, 1979, **NSRDS-NBS 61, Part II**.
42. S. R. Syeda, A. Afacan and K. T. Chuang, *Chem. Eng. Res. Des.*, 2004, **82**, 762-769.
43. D. Feng and C. Aldrich, *Ind. Eng. Chem. Res.*, 1999, **38**, 4110-4112.
44. B. B. Maini and V. Ma, *J. Canad. Pet. Technol.*, 1986, **25**, 65-69.
45. E. Tyrode, A. Pizzino and O. J. Rojas, *Rev. Sci. Instr.*, 2003, **74**, 2925-2932.
46. J.-M. Tarascon and M. Armand, *Nature*, 2001, **414**, 359-367.
47. H. Maekawa, M. Matsuo, H. Takamura, M. Ando, Y. Noda, T. Karahashi and S.-I. Orimo, *J. Am. Chem. Soc.*, 2009, **131**, 894-895.
48. M. Matsuo, A. Remhof, P. Martelli, R. Caputo, M. Ernst, Y. Miura, T. Sato, H. Oguchi, H. Maekawa, H. Takamura, A. Borgschulte, A. Züttel and S. Orimo, *J. Am. Chem. Soc.*, 2009, **131**, 16389-16391.
49. A. V. Skripov, A. V. Soloninin, M. B. Ley, T. R. Jensen and Y. Filinchuk, *J. Phys. Chem. C*, 2013, **117**, 14965-14972.
50. H. I. Schlesinger and H. C. Brown, *J. Am. Chem. Soc.*, 1940, **62**, 3429-3435.
51. A. Züttel, S. Rentsch, P. Fischer, P. Wenger, P. Sudan, P. Mauron and C. Emmenegger, *J. Alloys Compd.*, 2003, **356–357**, 515-520.
52. S.-I. Orimo, Y. Nakamori, N. Ohba, K. Miwa, M. Aoki, S.-i. Towata and A. Zuttel, *Appl. Phys. Lett.*, 2006, **89**, 021920-021923.
53. P. Mauron, F. Buchter, O. Friedrichs, A. Remhof, M. Bielmann, C. N. Zwicky and A. Zuttel, *J. Phys. Chem. B*, 2008, **112**, 906-910.
54. S. Orimo, Y. Nakamori, G. Kitahara, K. Miwa, N. Ohba, S. Towata and A. Zuttel, *J. Alloys Compd.*, 2005, **404-406**, 427-430.
55. D. S. Stasinevich and G. A. Egorenko, *Russ. J. Inorg. Chem.*, 1968, **13**, 341-343.
56. P. Martelli, R. Caputo, A. Remhof, P. Mauron, A. Borgschulte and A. Züttel, *J. Phys. Chem. C*, 2010, **114**, 7173-7177.
57. V. N. Konoplev and V. M. Bakulina, *Bull. Acad. Sci. USSR Div. Chem. Sci.*, 1971, **20**, 136-138.
58. W. I. F. David, S. K. Callear, M. O. Jones, P. C. Aeberhard, S. D. Culligan, A. H. Pohl, S. R. Johnson, K. R. Ryan, J. E. Parker, P. P. Edwards, C. J. Nuttall and A. Amieiro-Fonseca, *Phys. Chem. Chem. Phys.*, 2012, **14**, 11800-11807.
59. J. Gu, M. Gao, H. Pan, Y. Liu, B. Li, Y. Yang, C. Liang, H. Fu and Z. Guo, *Energy Env. Sci.*, 2013, DOI: 10.1039/C1032EE24121H
60. J.-H. Kim, S.-A. Jin, J.-H. Shim and Y. W. Cho, *J. Alloys Compd.*, 2008, **461**, L20-L22.
61. H.-S. Lee, Y.-S. Lee, J.-Y. Suh, M. Kim, J.-S. Yu and Y. W. Cho, *J. Phys. Chem. C*, 2011, **115**, 20027-20035.
62. M. D. Riktor, Y. Filinchuk, P. Vajeeston, E. G. Bardají, M. Fichtner, H. Fjellvag and M. H. Sørby, *J. Mater. Chem.*, 2011, **21**, 7188-7193.
63. Y. Yan, A. Remhof, P. Mauron, D. Rentsch, Z. Łodziana, Y.-S. Lee, H.-S. Lee, Y. W. Cho and A. Züttel, *J. Phys. Chem. C*, 2013.
64. I. Llamas-Jansa, O. Friedrichs, M. Fichtner, E. G. Bardaji, A. Züttel and B. C. Hauback, *J. Phys. Chem. C*, 2012, **116**, 13472-13479.
65. R. Černý, N. Penin, H. Hagemann and Y. Filinchuk, *J. Phys. Chem. C*, 2009, **113**, 9003-9007.
66. R. Liu, D. Reed and D. Book, *J. Alloys Compd.*, 2012, **515**, 32-38.
67. R. A. Varin, L. Zbroniec, M. Polanski, Y. Filinchuk and R. Černý, *Int. J. Hydrogen Energy*, 2012, **37**, 16056-16069.
68. M. Adams Roy, in *BORAX TO BORANES*, American Chemical Society, 1961, vol. 32, ch. 8, pp. 60-68.
69. K. N. Semenenko, A. P. Chavgun and V. N. Surov, *Russ. J. Inorg. Chem.*, 1971, **16**, 271-273.
70. R. L. Smith and J. W. Miser, *Compilation of the Properties of Lithium Hydride*, NASA Report: Technical Memorandum X-483, 1963.
71. E. A. Nickels, M. O. Jones, W. I. F. David, S. R. Johnson, R. L. Lowton, M. Sommariva and P. P. Edwards, *Angew. Chem. Int. Ed.*, 2008, **47**, 2817-2819.
72. H. Hagemann, V. D'Anna, J.-P. Rapin, R. Cerny, Y. Filinchuk, K. C. Kim, D. S. Sholl and S. F. Parker, *J. Alloys Compd.*, 2011, **509S**, S688-S690.
73. E. G. Bardají, Z. Zhao-Karger, N. Boucharat, A. Nale, M. J. van Setten, W. Lohstroh, E. Röhm, M. Catti and M. Fichtner, *J. Phys. Chem. C*, 2011, **115**, 6095-6101.
74. Z. Z. Fang, X. D. Kang, P. Wang, H. W. Li and S. I. Orimo, *J. Alloys Compd.*, 2010, **491**, L1-L4.
75. Z. Zhao-Karger, R. Witter, E. G. Bardaji, D. Wang, D. Cossement and M. Fichtner, *J. Mater. Chem. A*, 2013, **1**, 3379-3386.
76. J. Y. Lee, D. Ravnsbæk, Y.-S. Lee, Y. Kim, Y. Cerenius, J.-H. Shim, T. R. Jensen, N. H. Hur and Y. W. Cho, *J. Phys. Chem. C*, 2009, **113**, 15080-15086.

View Article Online
DOI: 10.1039/C3CP53920B

77. D. Blanchard, M. D. Riktor, J. B. Maronsson, H. S. Jacobsen, J. Kehres, D. Sveinbjörnsson, E. G. Bardají, A. Léon, F. Juranyi, J. Wuttke, B. C. Hauback, M. Fichtner and T. Vegge, *J. Phys. Chem. C*, 2010, **114**, 20249-20257.
78. Z. Z. Fang, X. D. Kang, J. H. Luo, P. Wang, H. W. Li and S. I. Orimo, *J. Phys. Chem. C*, 2010, **114**, 22736-22741.
79. Y.-S. Lee, Y. Filinchuk, H.-S. Lee, J.-Y. Suh, J. W. Kim, J.-S. Yu and Y. W. Cho, *J. Phys. Chem. C*, 2011, **115**, 10298-10304.
80. H.-S. Lee, S.-J. Hwang, H. K. Kim, Y.-S. Lee, J. Park, J.-S. Yu and Y. W. Cho, *J. Phys. Chem. Lett.*, 2012, **3**, 2922-2927.
81. L. Seballos, J. Z. Zhang, E. Rönnebro, J. L. Herberg and E. H. Majzoub, *J. Alloys Compd.*, 2009, **476**, 446-450.
82. G. F. Huff, *United States Patent*, 1960, **US 2,935,428**.